ACS APPLIED NANO MATERIALS

www.acsanm.org Article

# Luminescent Pressure-Sensitive Paints with Embedded Ag@$SiO_2$ Nanoparticles

Ji Feng, Colin W. Baxter, Igor V. Novosselov, Guozhong Cao, and Dana Dabiri*

Cite This: *ACS Appl. Nano Mater.* 2025, 8, 495−503 Read Online

ACCESS | Metrics & More | Article Recommendations | Supporting Information



**ABSTRACT:** Designing pressure-sensitive paint (PSP) to achieve high luminescence and high pressure sensitivity at near-atmospheric pressures increases the signal-to-noise ratio of the luminescence images, facilitating aerodynamic studies of low-speed flows. Here, we investigate a PSP formulation that incorporates silica-coated silver nanoparticles (Ag@$SiO_2$), along with Pt(II) *meso*-tetra(pentafluorophenyl)porphine (PtTFPP) embedded in a sol−gel matrix. The Ag@$SiO_2$ nanoparticles enhance the luminescence of PtTFPP by localized surface plasmon resonance (LSPR)-induced electric field enhancement rather than through altering the radiative decay rate of PtTFPP. The thickness of the silica layer and the mass ratio of Ag/PtTFPP are essential for optimizing the luminescence enhancement. In comparison to Ag-free PSP, the Ag@$SiO_2$-doped PSP exhibits a 2-fold luminescence enhancement while maintaining a high pressure sensitivity of 0.94%/kPa normalized to atmospheric pressure data. The high luminescence and pressure sensitivity not only offer increased signal strength for imaging low-speed airflows but also hold promising potential for future designs of PSP formulations using MEL.

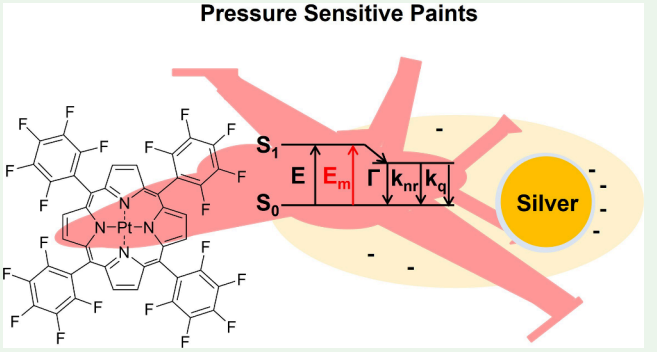


**KEYWORDS:** *metal-enhanced luminescence, plasmonic nanoparticles, thin film, oxygen sensing, pressure-sensitive paints*

## INTRODUCTION

Optical oxygen sensors have garnered widespread interest due to their high sensitivity and accuracy, lack of oxygen consumption, easy analysis over large surface areas, and full reversibility.[1] A notable application of these sensors is in pressure-sensitive paint (PSP), a surface pressure detection method that offers exceptional spatial resolution.[2,3] PSP has been applied to flight testing and wind tunnel experiments, benefiting both aircraft and automobile design.[4−6] It reduces the time and effort required to install a series of pressure taps, offering more sensing points to accurately map pressure across the entire surface.[7] Although commercially available PSP (UniFIB, ISSI) has a pressure sensitivity of 0.8%/kPa at 20 °C,[8] it is essential to have both increased absolute luminescent intensity near atmospheric pressures and improved pressure sensitivity (slope of the Stern−Volmer plot) to achieve superior resolution for low-speed aerodynamic measurements.

A typical PSP consists of oxygen-sensitive luminescent molecules (luminophores) imbedded in matrices.[9,10] When irradiated with light of specific wavelengths, the electrons of the luminophores are excited to higher electronic states and undergo either radiative decay or nonradiative decay as they return to the ground states (Figure 1a). Radiative decay, which includes fluorescence and phosphorescence, depends on whether the light emission involves a rapid return from an excited singlet state (fluorescence) or a slower return from an

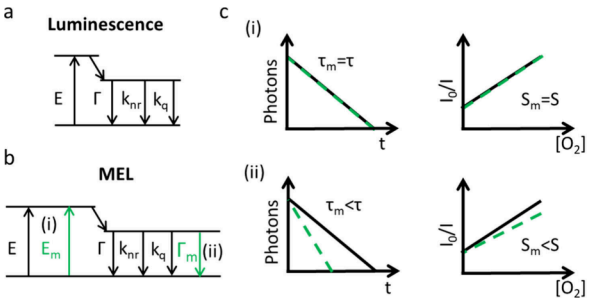


**Figure 1.** Illustration of (a) luminescence and (b) MEL by a modified Jablonski diagram. (i) and (ii) in (b) show MEL by increasing local electromagnetic field and radiative decay rate, respectively. (c) Lifetime and Stern−Volmer plots for (i) and (ii). The black lines and green dashed lines indicate those without and with MEL, respectively. $S$ is the slope of the Stern−Volmer plot for conventional PSP films, and $S_m$ is the slope of the Stern−Volmer plot for MEL-PSP films.

**Received:** October 16, 2024
**Revised:** December 5, 2024
**Accepted:** December 6, 2024
**Published:** December 20, 2024

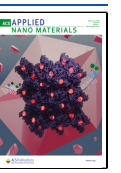





https://doi.org/10.1021/acsanm.4c05718
*ACS Appl. Nano Mater.* 2025, 8, 495−503

excited triplet state involving a spin change (phosphorescence), while nonradiative decay covers vibrational relaxation, internal conversion, and intersystem crossing.[11] Oxygen quenching happens when the excited luminophores collide with triplet oxygen molecules. During this process, the luminophores lose energy to the oxygen and return to the ground states, resulting in a reduction of luminescence. The quantum yield ($Q$) and luminescent lifetime ($\tau$) are described by eqs 1 and 2, which are functions of the radiative decay rate, $\Gamma$, the nonradiative decay rate, $k_{nr}$, and the oxygen quenching rate, $k_q$. The oxygen quenching rate is a product of bimolecular quenching rate ($\kappa_q$) and the oxygen concentration ($k_q = \kappa_q[O_2]$), where $\kappa_q$ primarily depends on the property of the matrices.[2,12] A Stern−Volmer plot is generated to correlate the photoluminescent intensity with the concentration of oxygen, as depicted in eq 3, where $I_0$ and $\tau_0$ denote the luminescent intensity and lifetime of a luminophore in the absence of oxygen, respectively. The slope of the Stern−Volmer plot, which is the product of $\tau_0$ and $\kappa_q$, reflects the pressure sensitivity of the film.[13] For aerodynamic applications, the luminescent intensity is usually normalized by the intensity value obtained at a known pressure ($P_{ref}$ in eq 4); for example, the pressure sensitivity of the commercial PSP UniFIB is obtained from the slope normalized by the intensity value at 100 kPa.

$$Q = \frac{\Gamma}{\Gamma + k_{nr} + k_q} = \frac{1}{1 + \frac{k_{nr} + k_q}{\Gamma}} \tag{1}$$

$$\tau = \frac{1}{\Gamma + k_{nr} + k_q} \tag{2}$$

$$\frac{I_0}{I} = \frac{\tau_0}{\tau} = \frac{\frac{1}{\Gamma + k_{nr}}}{\frac{1}{\Gamma + k_{nr} + k_q}} = 1 + \tau_0 \kappa_q [O_2] \tag{3}$$

$$\frac{I_{ref}}{I} = A(T) + B(T)\left(\frac{P}{P_{ref}}\right) \tag{4}$$

Enhancing the PSP performance by incorporating particles into the formulations has been a research focus. One approach is to add ceramic particles. For example, mesoporous silica hollow spheres increased the pressure sensitivity of Pt(II) *meso*-tetra(pentafluorophenyl)porphine (PtTFPP)/polystyrene films to 0.81%/kPa.[14] Similarly, $TiO_2$ submicron particles improved the luminescence of PtTFPP/poly[1-(trimethylsilyl)-1-propyne] films, although they also caused increased photodegradation.[15] Another approach to enhancing luminescence is metal-enhanced luminescence (MEL), achieved by incorporating plasmonic nanoparticles (NPs, e.g., Au, Ag, Cu, etc.) with luminophores, a technique that has been widely studied and applied in sensing and bioimaging fields.[16−21] The challenge with previous MEL-PSP lies in their inability to simultaneously achieve high sensitivity and enhanced luminescence. For example, Peak et al. reported an enhancement factor of 1.7 at 1 atm but with low pressure sensitivity ($I_0/I \sim 5$ at 20% $O_2$) by spraying luminophore and silica-coated Ag NPs.[22] Chu et al. reported the incorporation of Ag-coated silica NPs in a sol−gel matrix, resulting in increased pressure sensitivity ($I_0/I \sim 45$ at 20% $O_2$) but with reduced luminescent intensity by 75% at 1 atm.[23] In our previous studies, we also noticed a significant increase in pressure sensitivity upon the addition of metal NPs, while the actual luminescence intensity remained unchanged.[24,25]

The key to achieving both high pressure sensitivity and enhanced luminescent intensity at near-atmospheric pressure for MEL-PSP is to maximize the LSPR-induced electric field enhancement while preserving the quantum yield of the luminophore. The absolute fluorescence intensity ($I$) of the luminophore is composed of a near-field excitation rate ($\gamma_{ex}(\omega_{ex})$) and a quantum yield ($Q_{em}(\omega_{em})$) for far-field emission (eq 5):

$$I = \gamma_{ex}(\omega_{ex}) \times Q_{em}(\omega_{em}) \times \eta_{coll}(\omega_{em}) \times \sigma \tag{5}$$

where $\omega_{ex}$ and $\omega_{em}$ are the excitation and emission frequencies, respectively. $\eta_{coll}(\omega_{em})$ and $\sigma$ are collection efficiency and normalization factor, respectively, and will remain constant if the experimental setup is unchanged.[26] In MEL, upon excitation, the free electrons of the NPs oscillate strongly and generate localized surface plasmon resonance (LSPR). When a luminophore is near a plasmonic nanoparticle, the localized surface plasmon resonance (LSPR) peaks can match with either its absorption or emission spectra.[27−29] If alignment occurs with the absorption spectra, the LSPR increases the local electromagnetic field and boosts the luminophore's excitation rate (Figure 1b, route (i)). Conversely, if the overlap happens with the emission spectra, the coupling between the luminescence and the LSPR increases the radiative decay rate of the luminophore (Figure 1b, route (ii)).[20,30] This shows that either an increased local electromagnetic field or an enhanced radiative decay rate can boost the luminescence intensity at near-atmospheric pressures. However, the latter reduces the luminophore's lifetime (Figure 1c(ii)),[17,31,32] negatively impacting pressure sensitivity, and hence the slope of the Stern−Volmer plot ($S_m < S$). To avoid pressure sensitivity reduction, route (i) is preferred. The luminescence enhancement is achieved from electric field enhancement, while high pressure sensitivity can be attained by using highly porous binders. Additionally, when the luminophore is too close to the plasmonic NPs (<10 nm), the surface electrons on the NPs can interact with the luminophore, inducing an energy transfer from the excited luminophore to these surface electrons. The efficiency of this luminescence quenching is inversely proportional to the fourth power of the distance between the luminophore and the metal surface.[33] Simultaneously, the LSPR-induced electric field enhancement decreases exponentially as the luminophore moves away from the surface of the metal NP. Therefore, a spacer with an appropriate thickness must be created between the plasmonic NP and the luminophore to allow for the optimum separation that would maximize luminescence by balancing the fluorescence quenching and the electric field decay.[28,34−36]

The subject of this investigation is to fabricate MEL-PSP with both high pressure sensitivity and enhanced luminescence intensity at near-atmospheric pressures. We chose PtTFPP as the luminophore and a highly porous sol−gel matrix composed of three silica precursors to ensure high photostability and a large $\kappa_q$. To optimize MEL and pressure sensitivity, Ag NPs were chosen to match the absorption spectrum of PtTFPP. The Ag NPs were coated with a thin layer of silica to prevent particle aggregation and luminescence quenching of PtTFPP. Ag NPs of different particle and spacer sizes were synthesized and incorporated into the PSP to identify the optimal structure. The fluorescence enhancement factor was deter-


https://doi.org/10.1021/acsanm.4c05718
ACS Appl. Nano Mater. 2025, 8, 495−503

**Scheme 1. (a) Synthesis of Ag@$SiO_2$ NPs, Silica Sol, and the Molecular Structure of PtTFPP, (b) Film Fabrication via Spray Coating, and (c) Experimental Configuration for Luminescence and Stern–Volmer Plot Measurements**

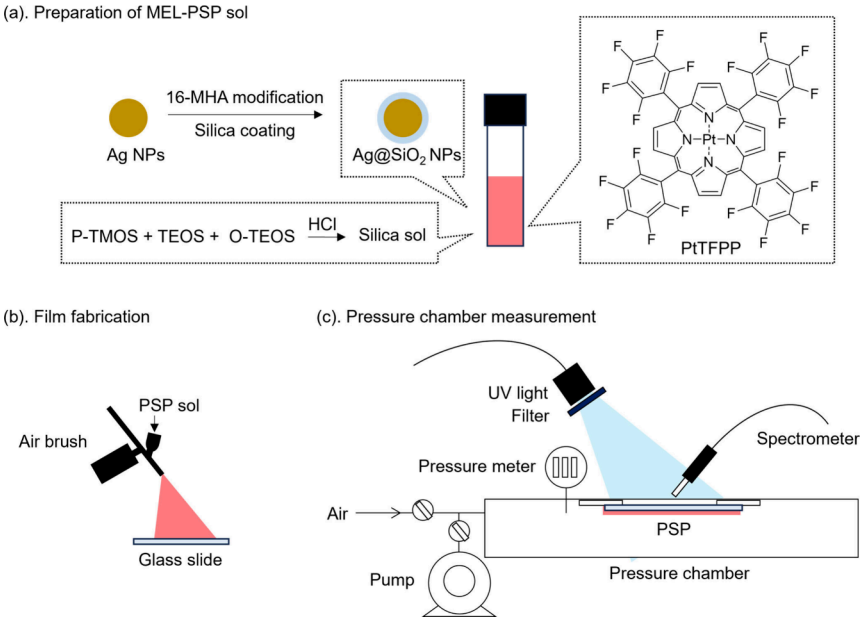


mined by the excitation and emission spectra of the PSP. Lifetime measurements confirmed the absence of any change in the decay rate, thus establishing the foundation for high pressure sensitivity.

## EXPERIMENTAL SECTION

**Chemicals.** Pt(II) *meso*-tetra(pentafluorophenyl)porphine (PtTFPP) and trimethoxy(propyl)silane (P-TMOS) were purchased from Fisher Scientific. Ethanol (EtOH) of proof 200 purity was purchased from Decon Labs. Tetrachloroauric(III) acid trihydrate ($HAuCl_4 \cdot 3H_2O$), silver nitrate ($AgNO_3$), polyvinylpyrrolidone (PVP, Mw = 40 000), acetonitrile (ACN), ascorbic acid (AA), triethoxy-(octyl)silane (O-TEOS), sodium borohydride ($NaBH_4$), tetraethyl orthosilicate (TEOS), hydrochloric acid (HCl), Triton X-100, 16-mercaptohexadecanoic acid (16-MHA), and diethylamine (DEA) were purchased from Sigma-Aldrich. All chemicals were used as received.

**Synthesis of Ag@$SiO_2$.** Ag NPs were synthesized by a seed-mediated growth.[37] The Au seeds were synthesized by adding 0.6 mL of freshly prepared $NaBH_4$ (0.1 M) solution into a mixture of 0.25 g of PVP, 10 $\mu$L of $HAuCl_4$ (0.25M), and 10 mL of $H_2O$ under vigorous stirring. The Au seeds were aged overnight to allow for the complete decomposition of $NaBH_4$.

The 95 nm Ag NPs were prepared by adding 6 mL of $H_2O$, 6 mL of PVP (5 wt %), 3 mL of ACN, 600 $\mu$L of AA (0. 1M), 0.9 $\mu$L of Au seed solution, and 450 $\mu$L of $AgNO_3$ (0.1 M). The mixture was stirred for 15 min at 27 °C to allow for the complete reduction of the Ag ions. The Ag NPs were then isolated by centrifugation at 5500 rpm for 10 min, washed with $H_2O$ twice, and redispersed in 12 mL of $H_2O$. Detailed recipes for the preparation of PVP-capped Ag NPs are shown in Table S2.

The Ag nanoparticles were modified with 16-MHA as a primer for silica coating.[38] The surface modification was achieved by adding 3.6 mL of 16-MHA (1 mM in ethanol) at a rate of 0.3 mL/min, followed by stirring for 30 min.[39] After surface modification, 7.8 mL of the 16-MHA-capped Ag NPs was mixed with 40 mL of ethanol and 1.5 mL of DEA and TEOS. The Ag@$SiO_2$ NPs were stirred for 1 h, isolated by centrifugation at 6000 rpm for 10 min, washed with ethanol twice, and redispersed in 10 mL of ethanol. The Ag element concentration in the final solution is calculated to be 2.25 mM.

**Fabrication of MEL-PSP.** The sol–gel matrix was made by mixing three silica precursors.[40] First, 2 mL of HCl (0.1 M) was added into a mixture of 0.88 mL of P-TMOS, 4 mL of TEOS, 2.15 mL of O-TEOS, and 6.25 mL of EtOH. After stirring for 1 h, 0.5 mL of Triton X-100 was added to the solution and stirred for 10 min.

For the preparation of MEL-PSP sol, different amounts of Ag NPs were isolated from the stock solution and redispersed in 200 $\mu$L of EtOH. Then, 0.5 mL of PtTFPP (0.2 mg/mL in EtOH) and 0.5 mL of the sol–gel matrix were added and stirred for 10 min. Then, 200 $\mu$L of the MEL-PSP sol was applied to a 12 × 12 mm glass slide by a gravity feed airbrush to achieve a uniform coating. Mild heating was used to accelerate solvent evaporation, resulting in uniform coatings. The sol was left to dry at room temperature (21 °C) for one day and was stored in the dark before measurement. A comparison of films prepared with and without mild heating is shown in Figure S3. The film prepared without mild heating developed nonuniformity, whereas the one prepared with mild heating appeared uniform. The glass slide was washed with ethanol and blow-dried before coating. No further treatments were needed.

The concentration of PtTFPP in the standard PSP formulation is 0.083 mg/mL; 2 mg/mL PtTFPP in the THF solution was used to prepare PSP with a higher concentration of PtTFPP.

To compare the pressure sensitivity, 200 $\mu$L of UniFIB (UF-25, ISSI, UN1263) was sprayed on a glass slide and left to dry at room temperature.

**Characterizations.** The structure of the Ag@$SiO_2$ NPs was imaged by using transmission electron microscopy (TEM, FEI Tecnai G2 F20 SuperTwin), operated at a 200 kV accelerating voltage. The extinction spectra of Ag@$SiO_2$ and PtTFPP were acquired using an Agilent Cary 60 UV–vis spectrometer. The film thickness was characterized using scanning electron microscopy (SEM, FEI Sirion XL30) at 5 kV and 25 pA. The cross-section of the film was coated with ~4 nm of platinum using a Leica EM ACE600 instrument. Fluorescence excitation spectra were measured using an Edinburgh FLS1000 system, equipped with a 450 W ozone-free xenon arc lamp and a Si PMT detector. Signals were measured at an emission wavelength of 656 nm. Luminescence lifetime measurements were conducted on the same instrument with a 405 nm ps pulsed diode laser and time-correlated single photon counting (TCSPC) electronics. A laser pulse of 10 $\mu$s was used. Photoluminescence and Stern–Volmer plots were measured in a pressure chamber equipped with a Kurt J. Lesker KJL276800LL digital pressure gauge, vacuum pumps, and gas valves (Scheme 1c). An OH36-24x11C UV lamp from LightSpeed Technologies Inc. with a 5-SB filter was used


https://doi.org/10.1021/acsanm.4c05718
ACS Appl. Nano Mater. 2025, 8, 495–503

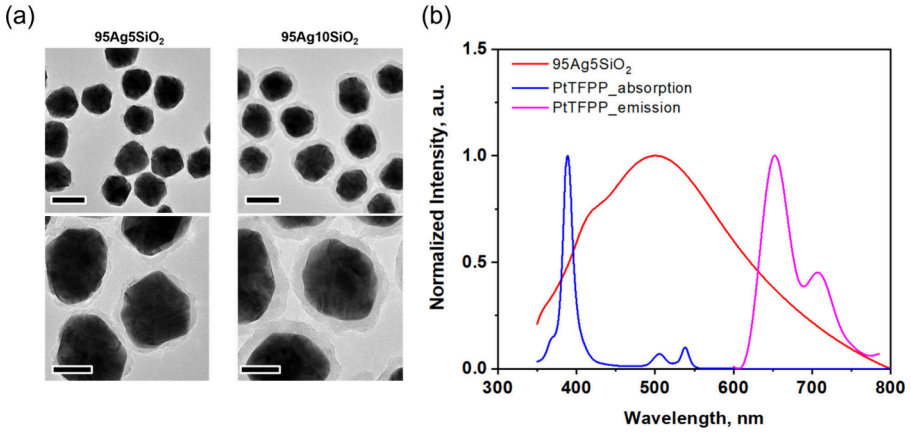


**Figure 2.** (a) TEM images of $95Ag5SiO_2$ and $95Ag10SiO_2$. (b) Extinction spectra of $95Ag5SiO_2$, absorption spectrum of PtTFPP, and emission spectrum measured with an excitation wavelength of 400 nm. The scale bars in (a) are 100 nm in the first row and 50 nm in the second row.

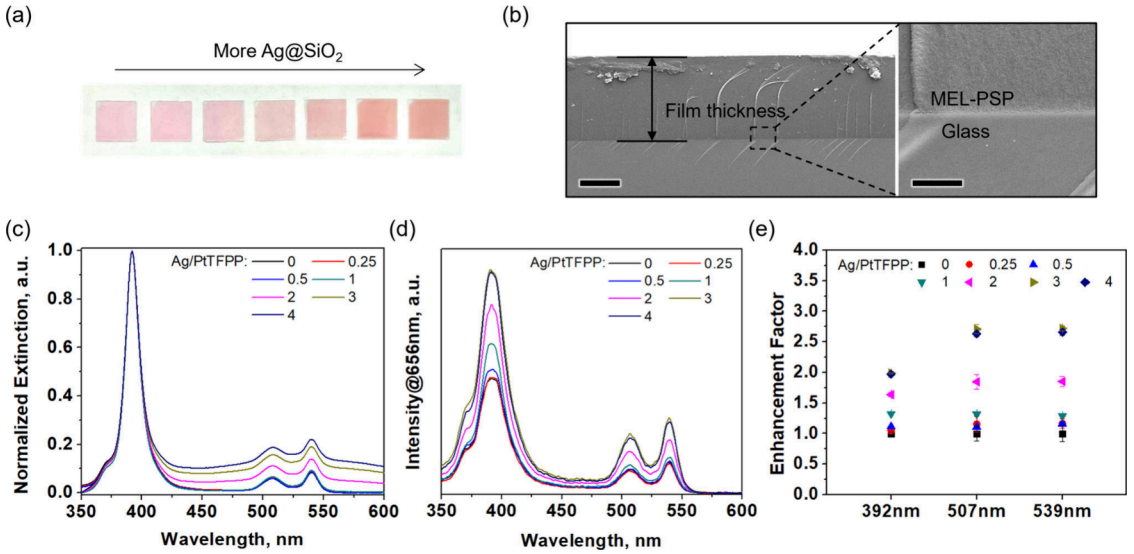


**Figure 3.** (a) Digital image of the MEL-PSP films. (b) SEM images of the cross-section for the MEL-PSP. The scale bars are 1 $\mu$m (left) and 500 nm (right). (c) UV−vis spectra of MEL-PSP films. (d) Excitation spectra of the MEL-PSP films measured at an emission wavelength of 656 nm. (e) Enhancement factor calculated at 392, 507, and 539 nm by the excitation spectra.

as the light source. The spectrum of the light source is shown in Figure S1. The luminescence was collected by optical fibers and analyzed by using an Ocean Optics spectrometer. Digital images of the PSP were taken by a JAI CV-M4 CL progressive scan camera with a Nikon AF Nikkor 50 mm 1:1.8 D lens. A 650 nm filter was mounted in front of the lens to eliminate light that was not luminescing. The spectrum representing the light transmitted through the filter is shown in Figure S2. The filter transmits light in the range of 585−700 nm. The final images were generated by averaging the results of 10 scans and then subtracting an average blank image without the sample.

## RESULTS

The MEL-PSP comprises PtTFPP and $Ag@SiO_2$ NPs dispersed in a sol−gel matrix (Scheme 1a), which is spray-coated on a glass slide (Scheme 1b) and dried. PtTFPP is a commonly used oxygen-sensitive metalloporphyrin due to the enhanced photostability resulting from fluorine substitution.[1] It exhibits a prominent Soret band at 392 nm along with two Q bands at 507 and 539 nm. Under UV excitation, it emits characteristic peaks at around 650 and 710 nm (Figure 2b). Ag NPs were chosen to enhance the fluorescence because the LSPR overlaps with the absorption spectrum of PtTFPP. This spectral alignment increases the electric field around the Ag NPs, thereby increasing the near-field excitation rate, $\gamma_{ex}(\omega_{ex})$, of PtTFPP. The Ag NPs were coated with a thin layer of silica to prevent particle aggregation and plasmonic quenching. The sol−gel matrix, formed with O-TMOS, P-TEOS, and TEOS, is highly porous ($I_0/I_{100} \sim 155$ in Table S1) comparing with other binders, allowing for fast oxygen quenching of PtTFPP. The $I_0/I$ was estimated to be 30 at 21% $O_2$.

We first compared the photoluminescence enhancement of MEL-PSP using PVP-modified Ag NPs with sizes of 19, 58, and 95 nm. As shown in Figure S4, 95 nm Ag NPs exhibit the greatest photoluminescence enhancement. TEM images of the $Ag@SiO_2$ NPs are shown in Figure 2a. The nanoparticles appear quasi-spherical due to the slow reduction kinetics resulting from the low seed concentration and the presence of PVP. The contribution of the Au seeds to the overall LSPR is negligible due to their small size and low quantity.[37] All NPs were dispersed in ethanol at a Ag concentration of 2.25 mM (0.243 mg/mL). We synthesized 16-MHA-modified 95 nm Ag nanoparticles and coated them with 0, 5, and 10 nm of silica, labeled as 95Ag, $95Ag5SiO_2$, and $95Ag10SiO_2$, respectively, in


https://doi.org/10.1021/acsanm.4c05718
ACS Appl. Nano Mater. 2025, 8, 495−503

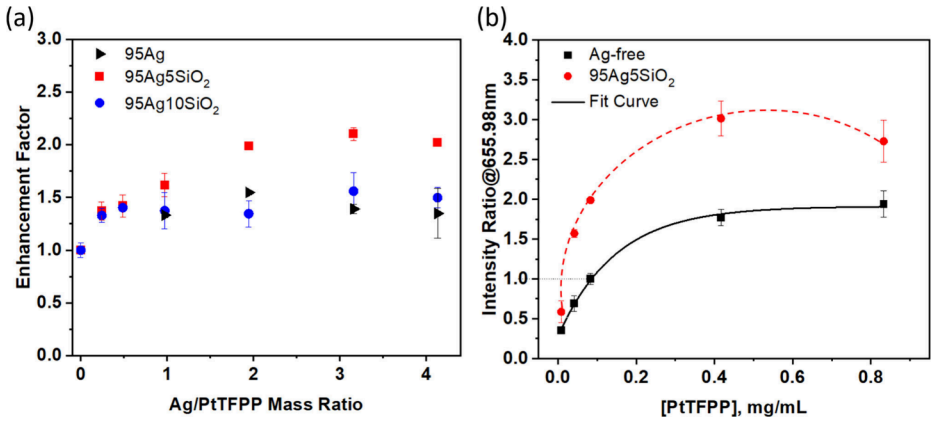


**Figure 4.** (a) Enhancement factor of 95Ag, 95Ag5$SiO_2$, and 95Ag10$SiO_2$. The mass ratios of Ag/PtTFPP are 0, 0.25, 0.5, 1, 2, 3, and 4. (b) Enhancement factor of PSP films with concentration of PtTFPP ranging from 0.0083 to 0.83 mg/mL. The black squares and red circles represent Ag-free films and 95Ag5$SiO_2$ of 0.166 mg/mL, respectively. The luminescence intensity of the Ag-free film with 0.083 mg/mL PtTFPP was used as a reference for normalization. The black line is an exponential fit of the black squares. The red dashed line is fit for the red dots.

order to determine the optimal spacer thickness. The extinction spectrum of 95Ag5$SiO_2$, ranging around 417 and 500 nm, aligns closely with the absorption peaks of PtTFPP (Figure 2b). The LSPR peak of 95Ag5$SiO_2$ is 150 nm blue-shifted from the emission peak of PtTFPP, indicating less favorable energy transfer between the plasmonic NP and the dye.

To optimize luminescence intensity, the amount of Ag NPs in the MEL-PSP film was adjusted to achieve Ag/PtTFPP mass ratios of 0.25, 0.5, 1, 2, 3, and 4. For comparison, a PSP film without Ag NPs was made by adding the same amount of ethanol to maintain the PtTFPP concentration. Figure 3a shows the PSP film with 95Ag5$SiO_2$. The Ag NPs are compatible with the sol−gel matrix, resulting in homogeneous films. The incorporation of 95Ag5$SiO_2$ results in a more pronounced coloration of the films. The film thickness was determined by imaging the cross-section of the MEL-PSP using SEM. As shown in Figure 3b, a distinct interface was observed between the MEL-PSP and the glass substrate. The thickness was calculated to be 22.3 ± 0.9 $\mu$m, based on the average of 10 measurements taken across the cross-section. Figure 3c shows the UV−vis spectra of the MEL-PSP films normalized by the intensity of the Soret peak. The increase of the extinction in the range of 400−600 nm is due to the LSPR of 95Ag5$SiO_2$.

We first measured the luminescence enhancement of the PSP films at atmospheric pressure by a standard method using a fluorometer. The excitation spectra of MEL-PSP were recorded at an emission wavelength of 656 nm (Figure 3d). The peak intensity increases as the Ag/PtTFPP ratio increases from 0 to 3 and slightly decreases when the Ag/PtTFPP reaches 4. To calculate the enhancement factor, the intensities of the peaks were recorded and normalized using the Ag-free PSP as a reference. The maximum luminescence enhancement, with enhancement factors of 2.0 and 2.7 achieved for the Soret band and Q bands, respectively, was attained when the Ag/PtTFPP ratio was equal to 3 (Figure 3e). The higher enhancement of the Q bands can be attributed to the better match of LSPR. The slight decrease in luminescence at Ag/PtTFPP = 4 may be due to the blocking of light by dense particles.

We then compared pressure chamber measurements with the fluorometer results to validate the reliability of our lab setup. For the pressure chamber measurements, the films were mounted at the same location of the pressure chamber and irradiated with the UV lamp. The intensity was recorded at 655.98 nm from the emission spectrum of each PSP film and normalized against the Ag-free PSP. The same trend present in the fluorometer results was observed with the pressure chamber measurements (Figure 4a, 95Ag5$SiO_2$). The highest enhancement factor of 2.1 was observed when the Ag/PtTFPP ratio was 3, which is in good agreement with the fluorometer measurements. These results demonstrate that although there are differences between the pressure chamber measurements and the fluorometer in terms of excitation light, irradiation area, and data collection, which may affect the absolute fluorescence intensity, these differences have a minimal impact on the measurement of the enhancement factor. In the Ag/PtTFPP = 3 case, the Ag content is as low as 0.25 mg/mL in the MEL-PSP formulation, indicating the high efficiency of the 95Ag5$SiO_2$ sample.

A proper spacer size between the metal and the luminophore is crucial for balancing luminescence quenching and electromagnetic field decay. Although the surface of the NPs is expected to undergo significant electric field enhancement, the occurrence of nonradiative charge transfer, leading to luminescence quenching, is also prominent in this scenario (Scheme 2). Förster resonance energy transfer (FRET) and

**Scheme 2. The Necessity of an Appropriate Spacer for MEL**

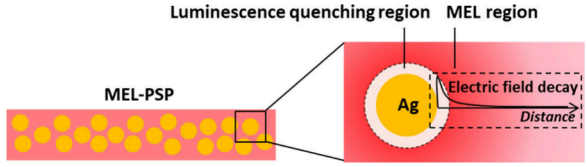


nanosurface energy transfer (NSET) are two key mechanisms that describe luminescence quenching on a metal surface. While FRET treats both the energy donor and acceptor as point dipoles, NSET approximates the metal NP as a collection of many point dipoles.[41,42] NSET suggests a quenching efficiency that is inversely proportional to the fourth power of the distance between the dye and the metal, a relationship that is supported by the majority of studies.[43] The optimal spacer sizes usually fall below 10 nm and vary depending on


https://doi.org/10.1021/acsanm.4c05718
ACS Appl. Nano Mater. 2025, 8, 495−503

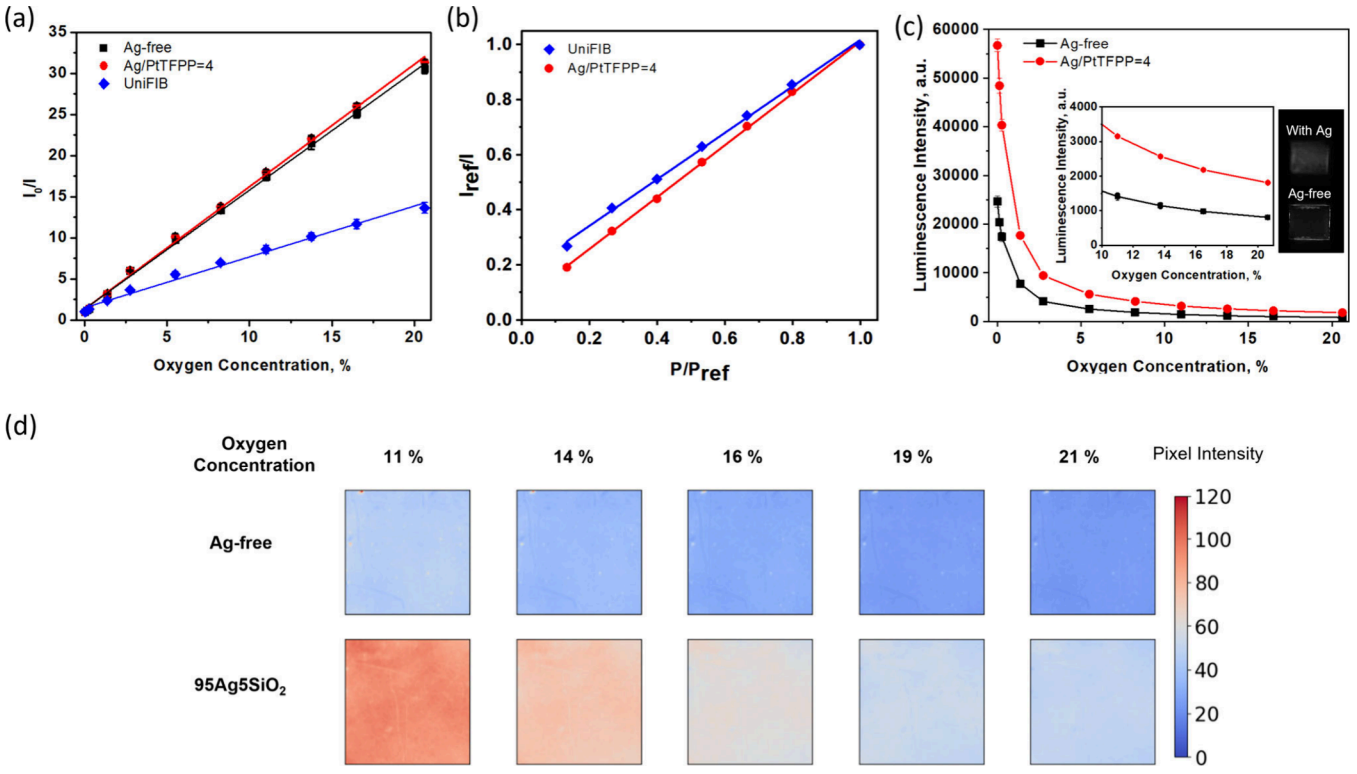


**Figure 5.** Stern−Volmer plots normalized by (a) intensity measured with 0.01% oxygen and (b) intensity measured at 1 atm of air at room temperature. (c) Absolute luminescence intensity plots of Ag-free PSP and 95Ag5$SiO_2$-incorporated MEL-PSP. The inset of (c) shows the zoomed-in absolute luminescence intensity plot and digital images of PSP with and without Ag NPs at 1 atm. (d) Images of PSP samples with different oxygen concentrations. The concentration of PtTFPP in the sol−gel film is 0.083 mg/mL.

specific cases.[44,45] Pan et al. observed substantial luminescence enhancement with a 3 nm spacer by coating PtOEP on silver NP films.[34] Yan et al. calculated the luminescence enhancement resulting from electric field enhancement and quantum yield modification of an FITC-loaded Ag@$SiO_2$ system, demonstrating that the optimal spacer size is 5 nm.[46] Another role of the spacer is to prevent NP aggregation. The 16-MHA-modified Ag NPs are not stable in the sol−gel matrix, as evidenced by a noticeable color change from yellow-gray to brown (Figure S5). Formation of Ag aggregates red-shifts the LSPR, increasing the likelihood of overlap with the emission wavelength of the dye and resulting in energy transfer.

The addition of silver NPs surpasses the phosphorescence intensity limit of the PSP film. It could be argued that the luminescence intensity of the PSP film can be enhanced by simply adding more PtTFPP. To verify this, we prepared Ag-free PSP films with different PtTFPP concentrations ranging from 0.0083 to 0.833 mg/mL. The intensity of the PSP luminescence was recorded and normalized by the intensity of the Ag-free film with 0.083 mg/mL PtTFPP (standard recipe). As shown in Figure 4b, the luminescence quickly increases in the low-concentration region before reaching a threshold. An exponential fit was performed, revealing the turning point around 0.2 mg/mL PtTFPP and a maximum luminescent enhancement of 1.9. Subsequently, another set of experiments were performed with 0.166 mg/mL 95Ag5$SiO_2$, revealing that this enhancement value can be achieved with just one-tenth of the PtTFPP. A luminescence enhancement factor of 3.0 can be achieved by combining 95Ag5$SiO_2$ with 0.416 mg/mL PtTFPP. It is also worth noting that a high content of the luminophore can cause self-quenching of the luminescence.[47,48] Therefore, using 95Ag5$SiO_2$ to implement MEL is an effective method for enhancing the luminescence of PtTFPP.

The 95Ag5$SiO_2$-incorporated MEL-PSP maintains the high pressure sensitivity of the sol−gel film. Its luminescence at 0.01% oxygen and room temperature was measured, and this value was used as $I_0$. As the oxygen concentration was increased by purging air into the pressure chamber, the luminescence intensity ($I$) decreased. Stern−Volmer plots were obtained by normalizing luminescence intensity at different oxygen concentrations with $I_0$. Both Ag-free PSP and 95Ag5$SiO_2$-incorporated MEL-PSP show highly linear plots (Figure 5a). The slopes of the Stern−Volmer plots were 1.446 and 1.488 for the Ag-free PSP and 95Ag5$SiO_2$-incorporated MEL-PSP, respectively. This slope is about 2 times that of the commercial PSP (UniFIB, Figure 5a, blue line). To compare their pressure sensitivity, the Stern−Volmer plots (Figure 5b) for the UniFIB and 95Ag5$SiO_2$-incorporated MEL-PSP were normalized to atmospheric pressure by using the intensity values in the pressure range from 13 to 100 kPa, respectively. The linear fit gives a pressure sensitivity of 0.94%/kPa ($R^2$ = 0.99935) for the MEL-PSP, which is 12% higher than that of the UniFIB (0.84%/kPa, $R^2$ = 0.99743). Further increasing the size of the Ag NPs to 150 nm results in matching of the LSPR peak and the emission of PtTFPP. As shown in Figure S7, while the photoluminescence enhancement factor near atmospheric pressure increases to 3.5, the pressure sensitivity decreases compared to the Ag-free PSP.

The absolute luminescence intensity plots show 2 times the fluorescence enhancement in the oxygen concentration range of 0.01−21% (Figure 5c). To further confirm the fluorescence


https://doi.org/10.1021/acsanm.4c05718
ACS Appl. Nano Mater. 2025, 8, 495−503

enhancement, we captured digital images of Ag-free PSP and 95Ag5$SiO_2$-incorporated MEL-PSP. A 650 nm filter was placed in front of the camera to collect the luminescence. The original grayscale images (Figure 5c, inset, and Figure S6) exhibit significant brightness enhancement of the 95Ag5$SiO_2$-incorporated MEL-PSP. Subsequently, the original images were processed to remove the dark background, after which a 100 × 100 pixel cropped image was extracted from the luminescent region. As shown in Figure 5d, 95Ag5$SiO_2$-incorporated MEL-PSP shows significantly higher pixel values compared to the Ag-free PSP. Specifically, the averaged pixel values for the 95Ag5$SiO_2$-incorporated MEL-PSP are 92, 73, 60, 52, and 49 for oxygen concentrations of 11%, 14%, 16%, 19%, and 21%, respectively. At each oxygen level, the 95Ag5$SiO_2$-incorporated MEL-PSP displays averaged pixel values that are twice as large as those of the Ag-free PSP. Notably, the averaged pixel value of the 95Ag5$SiO_2$-incorporated MEL-PSP at 21% oxygen concentration is comparable to that of the Ag-free PSP at 11% oxygen concentration.

Lastly, incorporating 95Ag5$SiO_2$ in the sol−gel PSP does not change the lifetime of PtTFPP. The luminescent decay was characterized by using a 10 $\mu$s pulse laser at 405 nm and 1 atm. The luminescent lifetime of UniFIB (Figure S8) was measured to validate the results, yielding a value of 4.21 $\mu$s, which is of the same magnitude as the value reported in previous studies.[49] As shown in Figure 6, the luminescence decay curves of MEL-

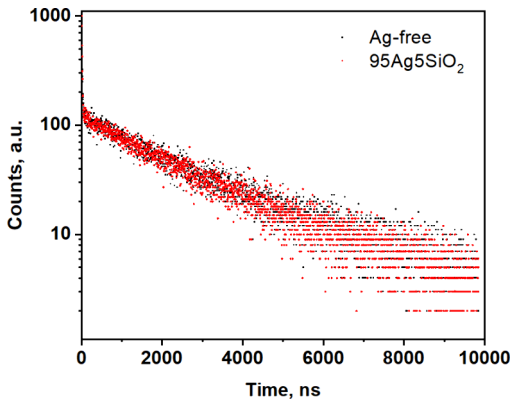


**Figure 6.** Luminescent decay of Ag-free PSP and 95Ag5$SiO_2$-incorporated MEL-PSP.

PSP and Ag-free PSP almost overlap each other. These curves exhibit a double exponential decay pattern described by the equation $y = A_1 \exp(-x/t_1) + A_2 \exp(-x/t_2) + y_0$. Further details, including the fitted line and parameter values, can be found in Figure S9 and Table S3. The average lifetime is 257 ns for both the Ag-free PSP and 95Ag5$SiO_2$-incorporated MEL-PSP. The unchanged lifetime indicates that the mechanism for MEL is electric field enhancement, not changing of the quantum yield. Similar observations have been reported with silica-coated gold NPs with PDI dyes, where the fluorescence lifetime remains unaltered for gold NPs coated with 7−13 nm silica shells.[50] The MEL-PSP exhibits good photostability, as demonstrated by the minimal change in fluorescence intensity after 20 min of continuous UV irradiation (Figure S10).

## CONCLUSION

In this work, we have successfully fabricated an MEL-PSP that has a high luminescence intensity and pressure sensitivity. Incorporating 95Ag5$SiO_2$ into PtTFPP and a sol−gel matrix results in a 2-fold luminescence enhancement compared to the Ag-free PSP, along with a pressure sensitivity of 0.94%/kPa normalized to atmospheric pressure data. Comparing with the literature, this is a notable improvement (Table S4). Notably, the MEL-PSP can even reach 3 times luminescence enhancement, surpassing what could be achieved solely by increasing the concentration of PtTFPP. The high luminescence intensity and pressure sensitivity stem from the LSPR-induced electric field enhancement. A key finding was that the Ag@$SiO_2$ NPs do not change the lifetime of PtTFPP, ensuring the maintenance of high pressure sensitivity. These advances in luminescence intensity and pressure sensitivity hold promise for an increased signal-to-noise ratio that will enhance the accuracy of pressure measurements in airflow applications. Future research in further designs of the nanoparticles can potentially enhance oxygen permeation in the binder, thereby resulting in a brighter and more sensitive film. Our insights into the mechanism of MEL-PSP will help for future advancements in PSP design and may receive broad interest in gas sensing applications.

## ASSOCIATED CONTENT

### Supporting Information

The Supporting Information is available free of charge at https://pubs.acs.org/doi/10.1021/acsanm.4c05718.

Spectrum of incident light, transmission spectrum of the 650 nm filter, results with PVP-modified 19, 58, and 95 nm Ag nanoparticles, digital images of PSP samples, results with 150 nm Ag nanoparticles, curve fit for luminescence lifetime, and tables for the preparation of Ag nanoparticles and fitting parameters for the fluorescence lifetime (PDF)

## AUTHOR INFORMATION

### Corresponding Author

**Dana Dabiri** − *Department of Aeronautics & Astronautics, University of Washington, Seattle, Washington 98195-2120, United States;* orcid.org/0000-0003-3573-6897; Email: dabiri@uw.edu

### Authors

**Ji Feng** − *Department of Aeronautics & Astronautics and Department of Mechanical Engineering, University of Washington, Seattle, Washington 98195-2120, United States;* orcid.org/0000-0002-9873-4840

**Colin W. Baxter** − *Department of Aeronautics & Astronautics, University of Washington, Seattle, Washington 98195-2120, United States*

**Igor V. Novosselov** − *Department of Mechanical Engineering, University of Washington, Seattle, Washington 98195-2120, United States;* orcid.org/0000-0002-6347-7450

**Guozhong Cao** − *Department of Materials Science & Engineering, University of Washington, Seattle, Washington 98195-2120, United States;* orcid.org/0000-0001-6539-0490

Complete contact information is available at: https://pubs.acs.org/10.1021/acsanm.4c05718

### Author Contributions

J.F. and D.D. developed and implemented the methodology. J.F. conducted all the experiments, analyzed data, and wrote



https://doi.org/10.1021/acsanm.4c05718
ACS Appl. Nano Mater. 2025, 8, 495−503

the manuscript. C.W.B. helped with pressure chamber measurements. D.D. revised the manuscript and supervised the work. I.V.N. provided access to facilities in which the experiments were performed. G.C. provided general guidance for this study.

### Notes

The authors declare no competing financial interest.

## ■ ACKNOWLEDGMENTS

The Airforce Office of Scientific Research (AFOSR) under Grant No. FA9550-23-1-0243 overseen by Dr. Gregg Abate financially supported this effort, for which we are grateful. Part of this work was conducted at the Molecular Analysis Facility, a National Nanotechnology Coordinated Infrastructure (NNCI) site at the University of Washington, which is supported in part by funds from the National Science Foundation (Awards NNCI-2025489 and NNCI-1542101), the Molecular Engineering & Sciences Institute, and the Clean Energy Institute. The authors acknowledge the use of facilities and instrumentation supported by the U.S. National Science Foundation through the UW Molecular Engineering Materials Center (MEM-C), a Materials Research Science and Engineering Center (DMR-2308979). The authors thank UW Molecular Analysis Facility staff members Ellen Lavoie for TEM assistance, Scott Braswell for SEM assistance, and UW MEM-C staff member Thom Snoeren for fluorometer assistance.

## ■ REFERENCES

(1) Wang, X.-D.; Wolfbeis, O. S. Optical methods for sensing and imaging oxygen: materials, spectroscopies and applications. *Chem. Soc. Rev.* **2014**, *43* (10), 3666−3761.
(2) Bell, J. H.; Schairer, E. T.; Hand, L. A.; Mehta, R. D. Surface pressure measurements using luminescent coatings. *Annu. Rev. Fluid Mech.* **2001**, *33* (1), 155−206.
(3) Liu, T.; Sullivan, J. P.; Asai, K.; Klein, C.; Egami, Y. In *Pressure and Temperature Sensitive Paints*; Springer, Cham, 2021.
(4) McLachlan, B. G.; Bell, J. H. Pressure-sensitive paint in aerodynamic testing. *Exp. Therm. Fluid Sci.* **1995**, *10* (4), 470−485.
(5) Houck, S. W.; Hepp, R. G.; Morris, M. J.; Benne, M. E. Pressure sensitive paint flight test. In *1996 IEEE Aerospace Applications Conference. Proceedings*; IEEE, 1996; pp 241−252.
(6) Gouterman, M.; Callis, J.; Dalton, L.; Khalil, G.; Mébarki, Y.; Cooper, K. R; Grenier, M. Dual luminophor pressure-sensitive paint: III. Application to automotive model testing. *Meas. Sci. Technol.* **2004**, *15* (10), 1986−1994.
(7) Kasai, M.; Sasaki, D.; Nagata, T.; Nonomura, T.; Asai, K. Frequency Response of Pressure-Sensitive Paints under Low-Pressure Conditions. *Sensors* **2021**, *21* (9), 3187.
(8) Ding, M.; Flaig, R. W.; Jiang, H.-L.; Yaghi, O. M. Carbon capture and conversion using metal−organic frameworks and MOF-based materials. *Chem. Soc. Rev.* **2019**, *48* (10), 2783−2828.
(9) Liu, T.; Campbell, B. T.; Burns, S. P.; Sullivan, J. P. Temperature- and Pressure-Sensitive Luminescent Paints in Aerodynamics. *Appl. Mech. Rev.* **1997**, *50* (4), 227−246.
(10) Jordan, J.; Watkins, A.; Weaver, W.; Dale, G.; Navarra, K. Sol-gel-based pressure-sensitive paint development. In *37th Aerospace Sciences Meeting and Exhibit*; AIAA, 1999.
(11) Itoh, T. Fluorescence and Phosphorescence from Higher Excited States of Organic Molecules. *Chem. Rev.* **2012**, *112* (8), 4541−4568.
(12) Gouterman, M. Oxygen Quenching of Luminescence of Pressure Sensitive Paint for Wind Tunnel Research. *J. Chem. Educ.* **1997**, *74* (6), 697.
(13) Gregory, J. W.; Sakaue, H.; Liu, T.; Sullivan, J. P. Fast Pressure-Sensitive Paint for Flow and Acoustic Diagnostics. *Annu. Rev. Fluid Mech.* **2014**, *46* (1), 303−330.
(14) Peng, D.; Gu, F.; Li, Y.; Liu, Y. A novel sprayable fast-responding pressure-sensitive paint based on mesoporous silicone dioxide particles. *Sens. actuators. A Phys.* **2018**, *279*, 390−398.
(15) Wu, J.; Huang, Z.; Kong, D.; Huang, F. Polymer-ceramic pressure-sensitive paint with high pressure sensitivity and pressure-sensitivity constancy in low-pressure environments. *Sens. actuators. A Phys.* **2024**, *366*, 114900.
(16) Su, Y.-Z.; Hung, M.-W.; Wu, W.-H.; Huang, K.-C.; Chiang, H. K. Application of metal-enhanced fluorescence technology in evanescent wave fluorescent biosensor. In *2010 IEEE Instrumentation & Measurement Technology Conference Proceedings*; IEEE, 2010; pp 574−578.
(17) Khurana, K.; Jaggi, N. Localized Surface Plasmonic Properties of Au and Ag Nanoparticles for Sensors: a Review. *Plasmonics* **2021**, *16* (4), 981−999.
(18) Tam, F.; Goodrich, G. P.; Johnson, B. R.; Halas, N. J. Plasmonic Enhancement of Molecular Fluorescence. *Nano Lett.* **2007**, *7* (2), 496−501.
(19) Sugawa, K.; Tamura, T.; Tahara, H.; Yamaguchi, D.; Akiyama, T.; Otsuki, J.; Kusaka, Y.; Fukuda, N.; Ushijima, H. Metal-Enhanced Fluorescence Platforms Based on Plasmonic Ordered Copper Arrays: Wavelength Dependence of Quenching and Enhancement Effects. *ACS Nano* **2013**, *7* (11), 9997−10010.
(20) Joyce, C.; Fothergill, S. M.; Xie, F. Recent advances in gold-based metal enhanced fluorescence platforms for diagnosis and imaging in the near-infrared. *Mater. Today Adv.* **2020**, *7*, 100073.
(21) Fothergill, S. M.; Joyce, C.; Xie, F. Metal enhanced fluorescence biosensing: from ultra-violet towards second near-infrared window. *Nanoscale* **2018**, *10* (45), 20914−20929.
(22) Peak, S. M.; Watkins, A. N. Addition of Silica-Coated Ag Nanoparticles to Enhance Luminescence Intensity of Pressure-Sensitive Paints. *ACS Appl. Nano Mater.* **2020**, *3* (10), 9813−9821.
(23) Chu, C.-S.; Sung, T.-W.; Lo, Y.-L. Enhanced optical oxygen sensing property based on Pt(II) complex and metal-coated silica nanoparticles embedded in sol−gel matrix. *Sens. Actuators, B* **2013**, *185*, 287−292.
(24) Yin, W.; Chen, J.; Sui, J.; Dabiri, D.; Cao, G. Luminescence and sensitivity enhancement of oxygen sensors through tuning the spectral overlap between luminescent dyes and SiO2@Ag nanoparticles. *Nano Select* **2021**, *2* (12), 2451−2460.
(25) Yin, W.; Sui, J.; Cao, G.; Dabiri, D. Silica Nanoparticles Coated with Smaller Au Nanoparticles for the Enhancement of Optical Oxygen Sensing. *ACS Appl. Nano Mater.* **2021**, *4* (12), 14146−14152.
(26) Chen, Y.; Munechika, K.; Ginger, D. S. Dependence of Fluorescence Intensity on the Spectral Overlap between Fluorophores and Plasmon Resonant Single Silver Nanoparticles. *Nano Lett.* **2007**, *7* (3), 690−696.
(27) Takeshima, N.; Sugawa, K.; Tahara, H.; Jin, S.; Wakui, H.; Fukushima, M.; Tokuda, K.; Igari, S.; Kanakubo, K.; Hayakawa, Y.; Katoh, R.; Takase, K.; Otsuki, J. Plasmonic Silver Nanoprism-Induced Emissive Mode Control between Fluorescence and Phosphorescence of a Phosphorescent Palladium Porphyrin Derivative. *ACS Nano* **2019**, *13* (11), 13244−13256.
(28) Kim, Y.; Kang, B.; Ahn, H.-Y.; Seo, J.; Nam, K. T. Plasmon Enhanced Fluorescence Based on Porphyrin−Peptoid Hybridized Gold Nanoparticle Platform. *Small* **2017**, *13* (26), 1700071.
(29) Geddes, C. D. Metal-enhanced fluorescence. *Phys. Chem. Chem. Phys.* **2013**, *15* (45), 19537−19537.
(30) Semeniak, D.; Cruz, D. F.; Chilkoti, A.; Mikkelsen, M. H. Plasmonic Fluorescence Enhancement in Diagnostics for Clinical Tests at Point-of-Care: A Review of Recent Technologies. *Adv. Mater.* **2023**, *35* (34), 2107986.
(31) Li, J.-F.; Li, C.-Y.; Aroca, R. F. Plasmon-enhanced fluorescence spectroscopy. *Chem. Soc. Rev.* **2017**, *46* (13), 3962−3979.
(32) Lakowicz, J. R. Radiative Decay Engineering: Biophysical and Biomedical Applications. *Anal. Biochem.* **2001**, *298* (1), 1−24.


https://doi.org/10.1021/acsanm.4c05718
ACS Appl. Nano Mater. 2025, 8, 495−503

(33) Su, Q.; Jiang, C.; Gou, D.; Long, Y. Surface Plasmon-Assisted Fluorescence Enhancing and Quenching: From Theory to Application. *ACS Appl. Bio Mater.* **2021**, *4* (6), 4684−4705.
(34) Pan, S.; Rothberg, L. J. Enhancement of Platinum Octaethyl Porphyrin Phosphorescence near Nanotextured Silver Surfaces. *J. Am. Chem. Soc.* **2005**, *127* (16), 6087−6094.
(35) Sun, J.; Li, Z.; Sun, Y.; Zhong, L.; Huang, J.; Zhang, J.; Liang, Z.; Chen, J.; Jiang, L. Uniform and reproducible plasmon-enhanced fluorescence substrate based on PMMA-coated, large-area Au@Ag nanorod arrays. *Nano Res.* **2018**, *11* (2), 953−965.
(36) Khatua, S.; Paulo, P. M. R.; Yuan, H.; Gupta, A.; Zijlstra, P.; Orrit, M. Resonant Plasmonic Enhancement of Single-Molecule Fluorescence by Individual Gold Nanorods. *ACS Nano* **2014**, *8* (5), 4440−4449.
(37) Liu, X.; Yin, Y.; Gao, C. Size-Tailored Synthesis of Silver Quasi-Nanospheres by Kinetically Controlled Seeded Growth. *Langmuir* **2013**, *29* (33), 10559−10565.
(38) Zhang, Y.; Kong, X.; Xue, B.; Zeng, Q.; Liu, X.; Tu, L.; Liu, K.; Zhang, H. A versatile synthesis route for metal@SiO2 core−shell nanoparticles using 11-mercaptoundecanoic acid as primer. *J. Mater. Chem. C* **2013**, *1* (39), 6355−6363.
(39) Gao, C.; Hu, Y.; Wang, M.; Chi, M.; Yin, Y. Fully Alloyed Ag/Au Nanospheres: Combining the Plasmonic Property of Ag with the Stability of Au. *J. Am. Chem. Soc.* **2014**, *136* (20), 7474−7479.
(40) Chu, C.-S.; Lo, Y.-L. Highly sensitive and linear calibration optical fiber oxygen sensor based on Pt(II) complex embedded in sol−gel matrix. *Sens. Actuators, B* **2011**, *155* (1), 53−57.
(41) Algar, W. R.; Hildebrandt, N.; Vogel, S. S.; Medintz, I. L. FRET as a biomolecular research tool — understanding its potential while avoiding pitfalls. *Nat. Methods* **2019**, *16* (9), 815−829.
(42) Chen, C.; Hildebrandt, N. Resonance energy transfer to gold nanoparticles: NSET defeats FRET. *Trends Anal. Chem.* **2020**, *123*, 115748.
(43) Hildebrandt, N.; Lim, M.; Kim, N.; Choi, D. Y.; Nam, J.-M. Plasmonic quenching and enhancement: metal−quantum dot nanohybrids for fluorescence biosensing. *Chem. Commun.* **2023**, *59* (17), 2352−2380.
(44) Anger, P.; Bharadwaj, P.; Novotny, L. Enhancement and Quenching of Single-Molecule Fluorescence. *Phys. Rev. Lett.* **2006**, *96* (11), 113002.
(45) Yang, J.; Zhang, F.; Chen, Y.; Qian, S.; Hu, P.; Li, W.; Deng, Y.; Fang, Y.; Han, L.; Luqman, M.; Zhao, D. Core-shell Ag@SiO2@mSiO2 mesoporous nanocarriers for metal-enhanced fluorescence. *Chem. Commun.* **2011**, *47* (42), 11618−11620.
(46) Yan, Y.; Meng, L.; Zhang, W.; Zheng, Y.; Wang, S.; Ren, B.; Yang, Z.; Yan, X. High-Throughput Single-Particle Analysis of Metal-Enhanced Fluorescence in Free Solution Using Ag@SiO2 Core−Shell Nanoparticles. *ACS Sens.* **2017**, *2* (9), 1369−1376.
(47) Grenoble, S.; Gouterman, M.; Khalil, G.; Callis, J.; Dalton, L. Pressure-sensitive paint (PSP): concentration quenching of platinum and magnesium porphyrin dyes in polymeric films. *J. Lumin.* **2005**, *113* (1), 33−44.
(48) Ruyten, W.; Sellers, M.; Baker, W. Spatially Nonuniform Self-Quenching of the Pressure-Sensitive Paint PtTFPP/FIB. In *47th AIAA Aerospace Sciences Meeting including The New Horizons Forum and Aerospace Exposition*; AIAA, 2009.
(49) Gouin, S.; Gouterman, M. Ideality of pressure-sensitive paint. II. Effect of annealing on the temperature dependence of the luminescence. *J. Appl. Polym. Sci.* **2000**, *77* (13), 2805−2814.
(50) Ribeiro, T.; Baleizão, C.; Farinha, J. P. S. Artefact-free Evaluation of Metal Enhanced Fluorescence in Silica Coated Gold Nanoparticles. *Sci. Rep.* **2017**, *7* (1), 2440.


https://doi.org/10.1021/acsanm.4c05718
*ACS Appl. Nano Mater.* 2025, 8, 495−503